Deep–Sea Research I 227 (2026) 104640

Contents lists available at ScienceDirect

Deep-Sea Research Part I

journal homepage: www.elsevier.com/locate/dsri

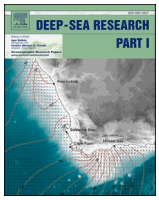

Evaluation of present-day hydrodynamic processes associated to the Belgica Mound contourite drift, offshore Ireland

Alice O. Matossian [a,*], Eoghan Daly [b,1], Sheena Fennell [b,2], Nadzeya Shymbaliova [a], Thomas Vandorpe [c], Martin White [b], David Van Rooij [a]

[a] Ghent University, Dept. of Geology, Campus Sterre, building S8, Krijgslaan 297, 9000, Gent, Belgium
[b] Earth and Life Science, School of Natural Sciences, University of Galway, University Road, Galway, H91 TK33, Ireland
[c] Flanders Marine Institute (VLIZ), Jacobsenstraat 1, 8400, Oostende, Belgium

ARTICLE INFO

Keywords:
Tidal currents
Small-scale bedforms
Moorings
Bottom currents
Porcupine seabight

ABSTRACT

The Belgica Mound Drift is a contourite drift located in the Porcupine Seabight, offshore Ireland, formed in association with cold-water coral mounds.

ROV imagery and bathymetry provided a close-up view of the drift seafloor, identifying multiple bedforms, including sinuous, linguoid and washed-out ripples as well as sediment waves. Three moorings equipped with current meters were deployed to better understand the spatial and temporal variations of the present-day hydrodynamic conditions over the drift moats and crest. Several velocity flows, ranging from 20 to 100 cm/s, were deduced from the interpretation of the bedforms and compared with the mooring-recorded flow values and character to evaluate the representativeness of the bedforms as a tool in the assessment of the strength and direction of bottom currents in deep environments. Both the tidally forced flows up to 50 cm/s, and the observed flow directions are consistent with the bedform estimation. While bedforms which require weaker bottom currents are currently formed during every tidal flow, the ripples created under stronger flows may be relic features formed during unrecorded peak flow events. This suggests that the drift and its moats are still being influenced by a strong hydrodynamic regime.

The spatial distribution of the bedforms suggests that the bottom current flow velocities are extremely variable, partly supported by the measured currents. This is likely related to the local topography which may have a very small spatial scale impact on the bottom flows.

1. Introduction

Hydrodynamic processes such as tides, bottom currents and internal waves shape the seafloor and enable the formation of erosional and depositional features (Besio et al., 2003). An example of these depositional features is represented by contourite drifts, occurring in shallow and deeper water settings ranging from hundreds of metres to several kilometres (Rebesco et al., 2014). On a smaller scale, hydrodynamic processes allow the development of bedforms that can give information about the strength, direction and variability of bottom currents (Hollister and Heezen, 1972; Kenyon and Belderson, 1973; Tucholke et al., 1985; Nelson et al., 1993; Wynn and Stow, 2002; Mulder et al., 2003; Masson et al., 2004; Hanquiez et al., 2007; Stow et al., 2009). However, due to a lack of thorough seafloor mapping and long-term hydrodynamic in-situ observations, little is known about bedform generation and dynamics in water depths beyond 100 m (Lo Iacono et al., 2020). Attempts, such as the bedform-velocity matrix developed by Stow et al. (2009), provide a first assessment of the present bottom current velocities and their spatial variability based on the observed type of bedforms.

The Belgica Mound Drift is an example of a deep-water small-scale contourite drift (50 km^2; 500–800 m water depth) located in the Belgica Mound Province, along the eastern slope of the Porcupine Seabight, offshore Ireland (Fig. 1; Matossian and Van Rooij, 2024). The drift is enclosed by cold-water coral (CWC) mounds and was created as a result of Quaternary glacial–interglacial cycles and the subsequent absence or

* Corresponding author.
E-mail address: alice.matossian@ugent.be (A.O. Matossian).
[1] Present address: Marine Institute, Rinville, Oranmore, Co. Galway, H91 R673, Ireland.
[2] Present address: P&O Maritime Logistics, Parkmore West Business Park, Co. Galway, H91 FW18, Ireland.

https://doi.org/10.1016/j.dsr.2025.104640
Received 25 June 2025; Received in revised form 6 October 2025; Accepted 10 December 2025
Available online 11 December 2025

presence of the Mediterranean Outflow Water (MOW) within the Porcupine Seabight (Matossian and Van Rooij, 2024). The formation of the drift is directly related to the interaction of the variable seabed topography with strong bottom currents, which are strengthened during interglacial periods and weakened during glacial periods (Matossian and Van Rooij, 2024). Additionally, these currents are crucial in the development of associated features, such as the CWC mounds (Van Rooij et al., 2003; Huvenne et al., 2009; Matossian and Van Rooij, 2024). The present-day area is affected by alongslope contour currents which are enhanced by trapped baroclinic diurnal tidal motions (White, 2007). Moreover, there is a local topographic intensification with the CWC mounds steering the bottom currents in their immediate surroundings (Van Rooij et al., 2007; Matossian and Van Rooij, 2024).

The Belgica Mound Province and more specifically the CWC mounds, such as the Challenger and Moira Mounds (Fig. 1), have been thoroughly examined in the past using high-resolution side-scan sonar (Wheeler et al., 2005; Huvenne et al., 2005) and ROV imagery (Foubert et al., 2005). During these surveys, many different types of large-scale features, demonstrating active sediment transport, have been identified such as striations, sand ribbons, barchan dunes, sediment waves and furrows (Foubert et al., 2005; Huvenne et al., 2005; Wheeler et al., 2005). The seafloor is typically made up of rippled sand with sediment waves and superimposed smaller-scale ripples representative of the general hydrodynamic conditions. According to Huvenne et al. (2005), the texture of the seafloor is rougher in the Belgica Mound Province than in the northern Porcupine Seabight areas, such as the Magellan and Hovland Mound Provinces. This is confirmed by Van Rooij et al. (2007) who indicated that the seafloor is composed of a coarse foraminiferal sand with moderate sorting and high sand content. The Belgica Mound Province is characterised by an irregular bathymetry with steep slopes of 2–3° (Huvenne et al., 2005). Past ROV observations reported a large number of dropstones next to the CWC mounds, associated with scours and gravel patches. All those earlier observations confirm the existence of local strong bottom currents with the CWC mounds acting as obstacles and steering the currents in their immediate surroundings (Wheeler et al., 2005; Foubert et al., 2005, 2011). Although these studies were crucial for understanding the current hydrodynamic regime in the area, they do not provide detailed information about the processes further away from the CWC mounds, specifically in a contourite drift context.

The latest seismic stratigraphy study of the contourite drift (Matossian and Van Rooij, 2024) suggests a heterogeneous depositional pattern, strongly influenced by the paleotopography and the CWC mounds. Strong alongslope bottom currents have been inferred in the moats, during the entire evolution of the drift, while the influence of the present-day hydrodynamic settings on the drift evolution remains difficult to entangle from seismic profiles alone. To improve comprehension of the lateral variability of the present-day bottom current pattern, a higher resolution view of the drift and its moats, such as with ROV imagery, is required. Based on an accurate bedform distribution and the use of the matrix of Stow et al. (2009), the recent hydrodynamic regime influencing this contourite drift can be investigated, and the current spatial architectural dynamics of the Belgica Mound Drift can be assessed (Fig. 1). The deployment of three moorings over the drift gives a great opportunity to define the temporal variability of the

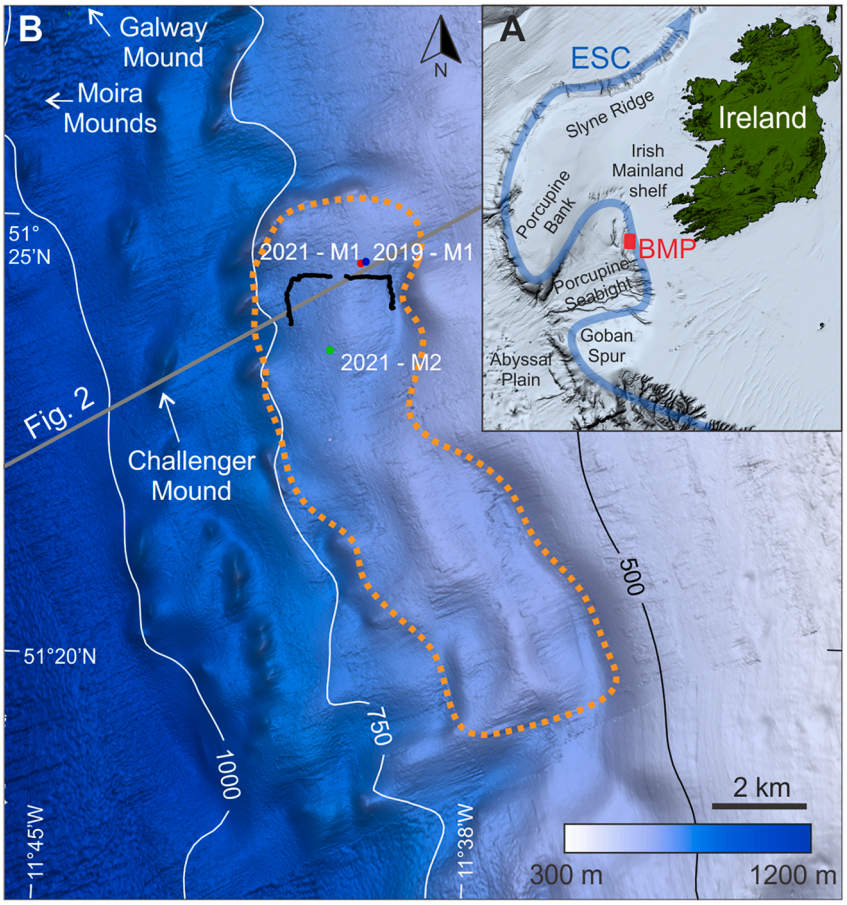

Fig. 1. (A) Regional map with the location of the Belgica Mound Drift within the Belgica Mound Province (BMP) (red rectangle) in the Porcupine Seabight, offshore Ireland. ESC stands for the European Slope Current. (B) Map of the study area with 20 m resolution bathymetry data acquired during the RV Belgica 2022/18 survey and 25 m resolution data (INFOMAR, 2023) in the background. The orange dotted line shows the extent of the Belgica Mound Drift. The grey line represents the salinity cross-section profile (Fig. 2). The mooring sites are circled in red, blue and green. The black line corresponds to the ROV track. (For interpretation of the references to colour in this figure legend, the reader is referred to the Web version of this article.)

hydrodynamic regime on a very local level. Moreover, these moorings allow to illustrate the representativeness of bottom current strengths and directions deduced from bedforms, by comparing them with the present-day recorded bottom currents. Consequently, this study aims (1) to identify the seafloor features, such as the bedforms and the seafloor texture, through the ROV imagery; (2) to evaluate the strength, the direction and the spatial variability of the bottom currents through the interpretation of the ROV observations and (3) to assess the temporal variability of the present-day near-seabed hydrodynamic regime through the analysis of the mooring datasets and verify the representativeness of the deduced bottom currents.

2. Regional setting

2.1. Geographic setting

Located 200 km west of Ireland, on the western margin of the Irish Shelf, the Porcupine Seabight is a large basin (320 × 240 km) with a N–S trend (Fig. 1) and water depth ranging from 350 m in the northern part to 3000 m in the southwest. The Irish Mainland Shelf borders this basin to the east, the Slyne Ridge and Porcupine Bank to the north, the Porcupine Ridge to the west and the Goban Spur to the south (Fig. 1). The basin opens out into the Porcupine Abyssal Plain towards the southwest (Naylor and Shannon, 1982).

2.2. Hydrographic setting

Within the study area (500–900 m water depth), a seasonal thermocline in the vicinity of the Belgica Mound Drift can be observed at a depth of 50–70 m (White, 2007). From 0 to 600 m water depth, the Eastern North Atlantic Water (ENAW; 10–12 °C; salinity range of 35.4–35.66) is present (Harvey, 1982; New et al., 2001; Rice et al., 1991; White, 2007). Between 600 and 800 m water depth, a permanent pycnocline separates the ENAW from the Mediterranean Outflow Water (MOW; 8–10 °C; salinity >35.5) (Pingree and Le Cann, 1990; Rice et al., 1991; van Aken and Becker, 1996; White, 2007). From 800 to 1000 m water depth, a salinity maximum is observed, which corresponds to the core of the MOW. The MOW has impacted the hydrodynamic regime in the Porcupine Seabight both in the past and the present (Dorschel et al., 2007; Huvenne et al., 2009). At present, the MOW flows steadily northwards from the Gibraltar Strait to the Porcupine Seabight (Iorga and Lozier, 1999; van Aken, 2000; McCartney and Mauritzen, 2001).

The general circulation in the Porcupine Seabight is cyclonic (White, 2007) and is influenced by the European Slope Current (500–2000 m water depth; Toucanne et al., 2021), with at its shallower levels the northward-flowing Shelf-Edge Current (Pingree and Le Cann, 1989). Along the NE Atlantic margin, the Shelf-Edge Current carries the upper part of the ENAW northward (Rice et al., 1991; New et al., 2001; White, 2007).

Along the NE Atlantic margin, there is an energy transfer from barotropic tides to baroclinic motions (Baines, 1974; White and Dorschel, 2010), including as examples, bottom trapped diurnal baroclinic waves and freely propagating semi-diurnal internal waves (White and Dorschel, 2010). Both these motions can be responsible for the amplification of bottom currents on the eastern flank of the Porcupine Seabight (Figs. 1 and 2) (White, 2007). It has been evidenced by White et al. (2007) that the enhanced K1 (diurnal) period baroclinic motions dominate the bottom current strength and direction around the Belgica Mound Province relative to the M2 (semi-diurnal) period tide. The trapped baroclinic motion can be rectified once it interacts with the seafloor, which allows the generation of a bottom current along the slope and a tidal bottom current. These alongslope and tidal bottom currents can be amplified under certain conditions (Huthnance, 1981; White and Dorschel, 2010), when a strong vertical density gradient, a permanent thermocline and a steep continental slope meet around the same water depth (600–800 m) (White, 2007; White and Dorschel, 2010). The local topography, including the CWC mounds, also plays a key role in the local variability and persistence of the bottom currents (White, 2007; Van Rooij et al., 2007). Associated to the Belgica Mound Drift area, the tidal bottom current crosses the slope while the alongslope bottom current follows the slope northwards (White et al., 2007).

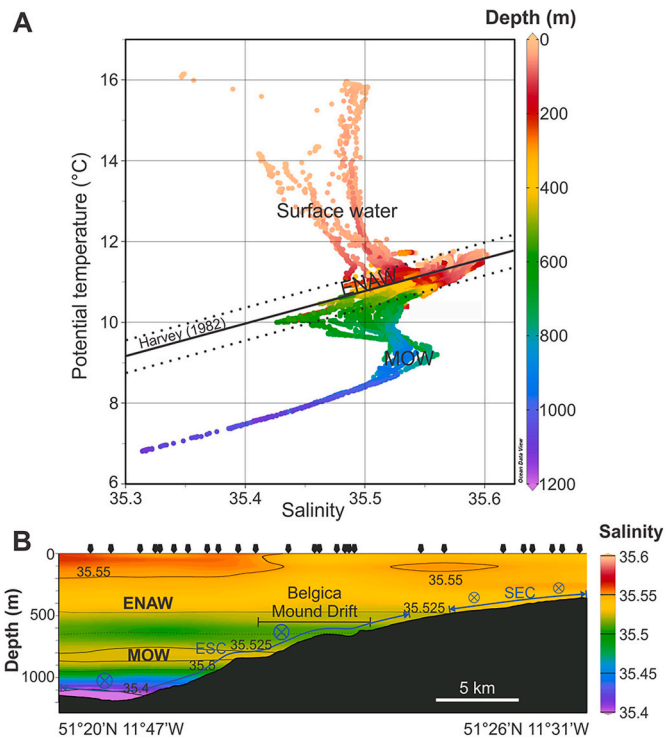

Fig. 2. (A) Temperature – salinity (T-S) diagram. The thick black line represents the characteristic T-S relationship of the ENAW as defined by Harvey (1982), while the dashed lines indicate a salinity variation of ±0.05 around this reference. (B) Salinity versus depth cross-section profile located over the study area (location: Fig. 1). A and B are based on CTD data (black arrows in panel B) from the World Ocean Database (Boyer et al., 2018) and were produced using Ocean Data View (Schlitzer, 2021). ENAW and MOW respectively stand for Eastern North Atlantic Water and Mediterranean Outflow Water. The dashed line shows the ENAW-MOW interface. The circled cross indicates the alongslope currents, European Slope Current (ESC) and Shelf-Edge Current (SEC), directed into the plane of the figure.

Mean persistent residual bottom currents, directed to the NW and thus following the continental slope, have been found to be between 1 and 7 cm/s (Pingree and Le Cann, 1990; White, 2007; Dorschel et al., 2009). Rice et al. (1991) have recorded speeds rarely exceeding 15 cm/s at 1 m above the seabed. However, significantly higher instantaneous velocities, with a SW-NE orientation and associated with diurnal tides, have been measured at the eastern edge of Porcupine Seabight, on the upper slopes and on top of Galway Mound (Fig. 1; Dorschel et al., 2007): Strong currents were measured, with peak velocities around 50–60 cm/s at 1 m above the seafloor (Dorschel et al., 2007). The observation of bedforms and current marks on top of and between the Belgica mounds indicates however that occasional stronger bottom currents prevailed (Foubert et al., 2005; Huvenne et al., 2009). Several types of current-induced bedforms have been formerly identified on high-resolution side-scan imagery on the eastern slope of the Porcupine Seabight, with some of them indicating a peak south-north alongslope current of up to 120 cm/s (Chachkine and Akhmetzhanov, 1998; Kenyon et al., 1998; Wheeler et al., 2000; Foubert et al., 2011).

2.3. Geological setting

With a Middle to Late Jurassic failed rift structure and features made

up of Precambrian rocks, deformed Upper Paleozoic strata, Mesozoic strata and a Cenozoic sediment cover on top, the bathymetry of the Porcupine Seabight demonstrates the complexity of the underlying geology (Naylor and Shannon, 1982). The basin is a deep sedimentary trough fault-bounded on its western and eastern margin and filled with post-rifts sediments with a thickness up to 10 km at its center (Naylor and Shannon, 1982).

Several major margin-wide erosive Cenozoic events have been identified in the Porcupine Seabight (McDonnell and Shannon, 2001). The most recent event is related to the reintroduction of the MOW in the Porcupine Seabight during the Late Pliocene (Stow, 1982; Pearson and Jenkins, 1986; Van Rooij et al., 2003, 2009). It was responsible for the RD1 unconformity (Van Rooij et al., 2003), on top of which the CWC mounds and the Belgica Mound Drift started to form (Matossian and Van Rooij, 2024). The peculiar RD1 paleotopography, still visible in the present-day bathymetry, as well as the CWC mounds, strongly influence the local hydrodynamic conditions and play a role in the onset and development of the contourite drift. The contourite drift was formed under persistent alongslope bottom currents since the Pleistocene (Matossian and Van Rooij, 2024). At a larger scale, the evolution of the drift is related to the Pleistocene glacial and interglacial cycles (Matossian and Van Rooij, 2024). During interglacial periods, the MOW enters the Porcupine Seabight, increasing the bottom current intensity, while during glacial periods, the MOW does not reach the basin, weakening the bottom currents (Huvenne et al., 2009; Raddatz et al., 2011) and allowing the sediment to accumulate on the drift (Matossian and Van Rooij, 2024). Since the lower Pliocene, the MOW is involved in the formation of large contourite depositional systems all along the NE Atlantic margin (Khélifi et al., 2009, 2014), which makes the Belgica Mound Drift one of the most distal contouritic expression of the MOW in the NE Atlantic Ocean.

3. Material and methods

Three moorings equipped with Aanderaa RCM7 current meters were used to assess the bottom current regime (Table 1). In the course of the RV Belgica 2019/16 survey, a short-term fixed bottom mooring 2019-M1 (Table 1) was set up and placed on the crest of the drift (Fig. 1). Two additional long-term moorings were deployed (Table 1) within the Belgica Special Area of Conservation designation during the Irish Marine Institute survey CE21014 in 2021. Both moorings were impacted by suspected trawling activity, leading to the loss of both near seabed (<10 m) current meters. While mooring 2021-M2 was deployed further south on the crest and recorded 20 days prior to experiencing a compass issue, 2021-M1 was deployed near the 2019 deployed mooring location and recorded for 6 months. The three deployed current meters were equipped with a Fenwall thermistor (temperature sensor). Vectors were measured every 1/50th of the sampling interval (Table 1). Data were processed and quality controlled using instrument-specific calibration data provided by Aanderaa and appropriate magnetic declination. Measured current speed and direction were converted to east and north velocity components. A simple least squares tidal analysis was performed over the full available time series.

During the RV Belgica 2019/16 survey, one ROV-dive was carried out using the Flanders Marine Institute's (VLIZ) ROV Zonnebloem (SubAtlantic Cherokee observation type). The transect, located in the northern sector of the drift (5 km^2, 2.5 × 2 km; Fig. 1) is 3.4 km long and covers parts of three main morphological elements of the contourite drift: its western and eastern moats (1 km and 900 m long respectively) and a transect crossing the crest (1.5 km long).

A multibeam echosounder BlueView M900-2250 Dual Frequency Series operating at a frequency of 900 kHz was installed on the ROV to acquire high-resolution bathymetry. The vertical resolution of the data is approximately 5 cm. The BlueView has 130° field of view and sends out 768 beams at 900 kHz. The data were roll and pitch corrected using the compass of the ROV (TCM2.6) and positioning data were obtained every 2 s using an iXBlue GAPS USBL positioning device. Sound velocity data were collected by a ROV-mounted Sea&Sun 48M-CTD. The bathymetric data were recorded in real time using Qinsy (QPS). Due to the low update rate of the positioning data, the lack of a depth sensor and Kalman filter, the bathymetric data appear stepwise along-transect. The HD video data were gathered using a Luxus HD camera that faced downward. Along the track, the ROV flew no higher than 5 m above the seafloor. During the dive, the ship moved as slow as possible (velocity <1 knot) along the transect.

The processing of the ROV bathymetric data was performed with Qimera 2.6.2 (QPS). A sound velocity correction was applied on each sonar file using the collected CTD data and the outliers were manually removed. The full analysis of the HD video, as well as the identification and the mapping of the observed seafloor features have been carried out with ArcMap 10.7.1 coupled with the Full Motion Video module. Screenshots of the video frames were taken during the mapping.

Processed 25 m resolution bathymetric data (Fig. 1) were also made available by INFOMAR (2023) and downloaded from the INFOMAR Marine Data Download Portal. Higher resolution bathymetric data over the drift have been acquired in 2022, using the Kongsberg EM 304 multibeam echosounder during the RV Belgica 2022/18 survey. The dataset has been processed with Qimera 2.6.2 (QPS) and exported with a 20 m resolution. The salinity data (Fig. 2) are based on CTD data from the World Ocean Database (Boyer et al., 2018) and were used for the identification of the water masses.

4. Results

4.1. Moorings

All current measurements showed similar characteristics for the bottom current regime (Table 2).

Table 2
Summary statistics for the three deployed mooring. The residual current is computed using a time-averaging method with a 30-h averaging window.

Mooring	Speed (cm/s)	East (cm/s)	North (cm/s)	Residual current Direction (°) and speed (cm/s)
2019-M1				
Mean	20.5	−1.1	−3.7	196.0 and 3.8
Maximum	52.8	51.3	28.3	/
Minimum	0.6	−39.8	−26.7	/
2021-M1				
Mean	14.9	−0.9	4.6	348.6 and 4.7
Maximum	42.7	42.4	24.3	/
Minimum	1.1	−37.6	−18.4	/
2021-M2				
Mean	14.6	0.7	7.9	5.4 and 7.4
Maximum	42.1	40.7	23.9	/
Minimum	1.1	−29.7	−19.6	/

Table 1
Summary of the characteristics of the deployed moorings. Water depth was obtained through INFOMAR (2023) bathymetry (Fig. 1).

Mooring	Latitude	Longitude	Water depth	Height current meter	Start date	Recording period	Sampling interval
2019-M1	51°24′N	11°39′W	636 m	6 m	06/06/19	8 days	10 min
2021-M1	51°24′N	11°39′W	632 m	35 m	05/06/21	180 days	30 min
2021-M2	51°23′N	11°40′W	655 m	35 m	05/06/21	20 days	30 min

The 2021 data yielded comparable results (Fig. 3A; Table 2): Taking a smaller subset of the longer 2021-M1 dataset coinciding with the 2021-M2 dataset indicates that the shorter 2021-M2 data was representative of the longer time series during the coincident measurement period. Currents were dominated by across-slope tidal periodicity and smaller residual alongslope flows (Fig. 3A). Peak tidally induced speeds were typically between 25 cm/s (neaps) to > 35 cm/s at spring tides, with a maximum speed of 40 cm/s (2021-M1) and 42 cm/s (2021-M2) respectively. Similarly, at both 2021-M1 and 2021-M2, mean flow speeds were similar (14.9 cm/s for 2021-M1 and 14.6 cm/s for 2021-M2; Table 2) with 2021-M1 having a mean of 15.6 cm/s for the comparable 2021-M2 time period. Residual currents were northward. At 2021-M1, there is a mean residual flow of 4.7 cm/s in direction 348.6°N and at 2021-M2, 7.4 cm/s in direction 5.4°N.

At the 2019-M1 location, characteristics are similar to the 2021 moorings with a tidally dominated across-slope bi-directional current (Fig. 3A, 3C) found in the short 8-day time period and a mean speed of 20.5 cm/s and maximum of 52.8 cm/s (Fig. 3A; Table 2). The residual flow of 3.8 cm/s is directed to the SW.

Rotary spectral and tidal analyses (Fig. 3B) identified the diurnal K_1 tide (23.93 h period) with the diurnal O_1 tide (25.82 h period) and semi-diurnal M_2 tide (12.42 h period) as the primary and secondary tidal constituents respectively, dominating the bottom currents at all moorings. At the 2021-M1 mooring (Fig. 3B), the diurnal O_1 tide was significant. The three tidal constituents have their major tidal ellipse axis directed across slope, with orientation and amplitudes of $K_1 = 88°$, 15.3 cm/s, $M_2 = 113°$, 6.9 cm/s and $O_1 = 82°$, 7.7 cm/s, respectively. The K_1 component is characterised by a strongly elongated, anti-clockwise rotary tidal ellipse (from the 2021-M1 timeseries), with M_2 and O_1 having clockwise rotary motion. A strong spring-neap cycle (Mf = 327 h) is also apparent in the timeseries. All mooring based temperature timeseries (Fig. 3C) show an asymmetrical pattern, with rapid temperature decrease correlated with upslope flow, followed by more gradual increase linked to downslope flows.

4.2. ROV bathymetry

Since the frequency of 900 kHz results in a 5 cm vertical resolution,

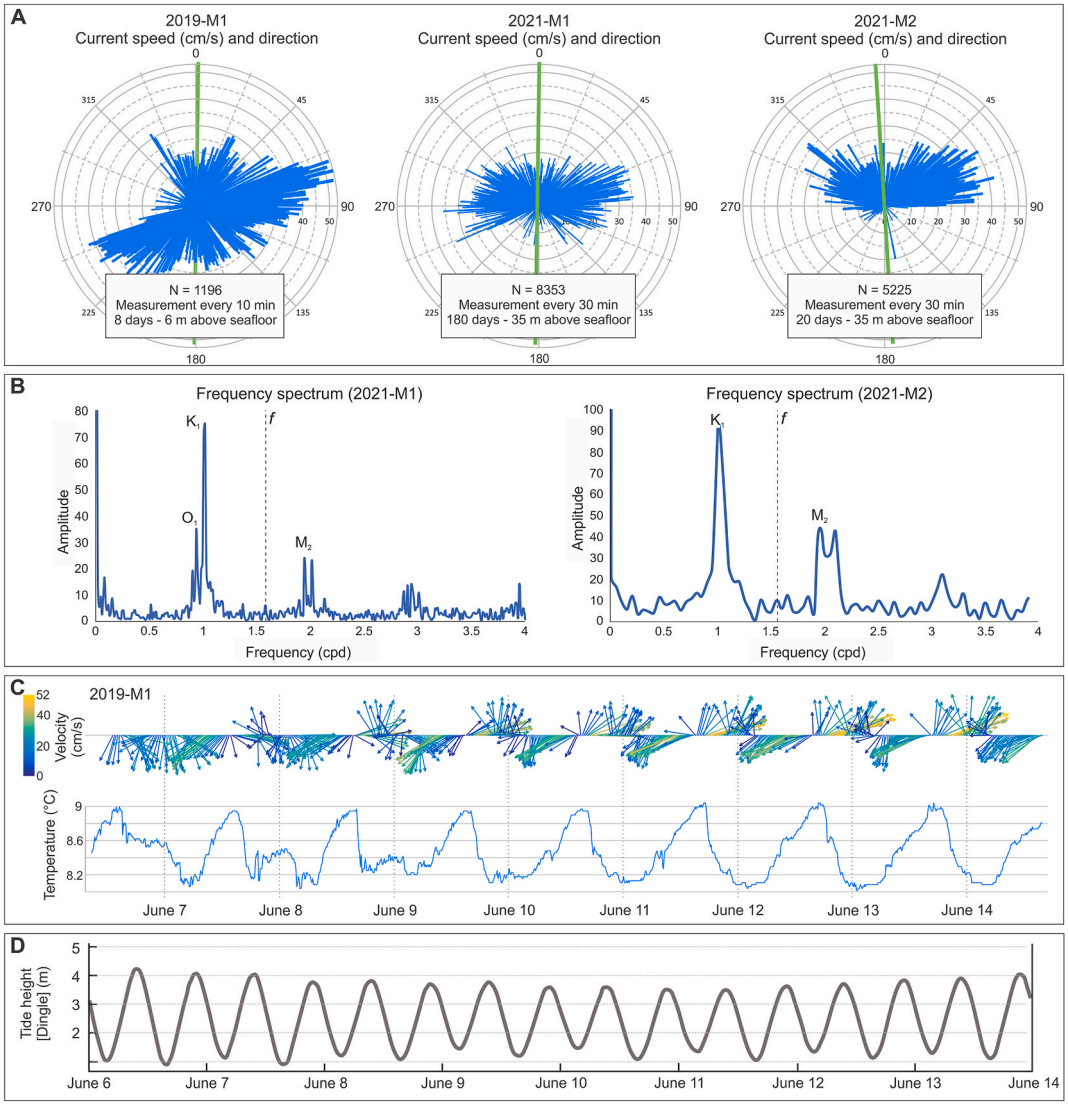

Fig. 3. (A) Rose diagrams with the measured current speed (x axis) and direction from the three moorings (location: Fig. 1). The green bar shows the drift crest orientation. To make the figure clearer, only one measurement out of every ten is displayed for mooring 2021 - M1. N corresponds to the number of measurements. (B) Frequency spectrum of tidal constituents in cycles per day (cpd) highlighting the dominant components for the 2019-M1, 2021-M1 and 2021-M2 moorings. The K_1, M_2 and O_1 tidal constituents, as well as the inertial frequency (f), are indicated. (C) Results from mooring 2019-M1 (location: Fig. 1), with the current vectors and temperature fluctuations at 6 m above the seafloor. (D) Tide height (m) recorded at Dingle during the deployment period (Marine Institute, 2019). (For interpretation of the references to colour in this figure legend, the reader is referred to the Web version of this article.)

the ROV bathymetric data are only suitable to describe bedforms exceeding 5 cm in height. Moreover, the update rate of the USBL positioning of the ROV and lack of Kalman filter caused steplike artefacts in the bathymetry data, which are visible as across-tracks lines on the bathymetry map (Fig. 4). Consequently, only across-track height differences exceeding 5 cm are reliable, as along-track height differences are most likely jumps in ROV latitude, longitude and/or altitude. Several NNW–SSE oriented sediment steps, with height differences of 5–40 cm, can be traced over 40–150 m along the western moat of the drift (Fig. 4, profile C-D).

4.3. ROV visual imagery

A variety of bedforms were observed over the crest and within the moats of the contourite drift. Following the bedform classification of Simons and Richardson (1966), as well as the bedform matrix of Stow et al. (2009), numerous features have been observed and identified. They have been classified into five categories (Fig. 5; Table 3).

(1) Straight to sinuous ripples (Fig. 5A–Table 3) are asymmetrical with a short and steep lee side and a gentler stoss side. They are straight to undulatory crested. The associated texture of the seafloor is generally among the roughest encountered with pebble to cobble-size clasts and less sorted (biogenic) mixed sand, predominantly accumulating in the ripple troughs.
(2) Washed-out ripples (Fig. 5B–Table 3) are smaller compared to the straight to sinuous ripples, with a shorter lee side. They appear to be planed off. They are associated with irregular gravel patches visible in the trough of the ripples. These patches are composed of poorly sorted coarser pebble to cobble-size clasts and some boulders.
(3) Linguoid ripples (Fig. 5D–Table 3) are asymmetrical with a steeper and shorter lee side compared to straight to sinuous ripples. They display a highly variable morphology with an irregular crescent-shaped crest. The seafloor texture is usually very fine and well-sorted with pale-coloured fine sand.
(4) Small-scale dropstones (Fig. 5B) are on average around 10 cm wide, but they can be up to 60 cm. Some are associated with scours and feature a gravel tail at the back. The gravel tails are 10–50 cm long and their orientations lie perpendicular to the surrounding ripple crests.
(5) Large-scale sediment steps (Fig. 5C–Table 3) are continuous straight ridges with an asymmetric profile. Their maximum height is 40 cm. They are ten to several tens of metres apart. They are characterised by a sharp, almost vertical drop. The steps are covered by smaller bedforms.

The observed ripple sequence is described in Fig. 5, ranging from deep (moat) to shallow (crest), in an upslope direction. Sinuous ripples (Fig. 5A) fade into washed-out ripples (Fig. 5B). Dropstones, as well as gravel patches are numerous in the washed-out ripple areas (Fig. 5B). Washed-out to sinuous ripples are observed at the foot of the sediment step (Fig. 5C). These ripples are mostly observed perpendicular or oblique to the crest orientation of the step while the linguoid ripples on top have the same orientation (Fig. 5D). Sometimes, the ripples at the foot of the step are parallel to the step crest alignment (Fig. 6a, 6b). Further upslope, the linguoid ripples merge into straight to sinuous ripples (Fig. 5E). Straight to sinuous as well as linguoid ripples do not show any sign of erosion. The same sequence is observed in reverse on the eastern ROV track.

Based on the ROV visual imagery, the spatial distribution of the observed bedforms along the ROV track was plotted as sedimentary bedform maps (Fig. 6). These display the small and large-scale bedform distribution, as well as the texture of the seafloor.

The boundaries between the bedform areas generally feature a NNW–SSE orientation and their transition may be rather sharp. Most bedform areas are only a few metres wide in the moats, but on the drift crest, they can reach several tens of metres (Fig. 6d). The sediment steps are only located within the western and eastern moats of the drift (Fig. 6a, 6b, 6c, 6e, 6f). No steps have been observed on the crest of the drift (Fig. 6d). They are typically 10–50 m apart in the western moat (Fig. 6a, 6b, 6c) and 10 m apart in the eastern moat (Fig. 6e), with an average NW–SE alongslope orientation. In total, 30 sediment steps have

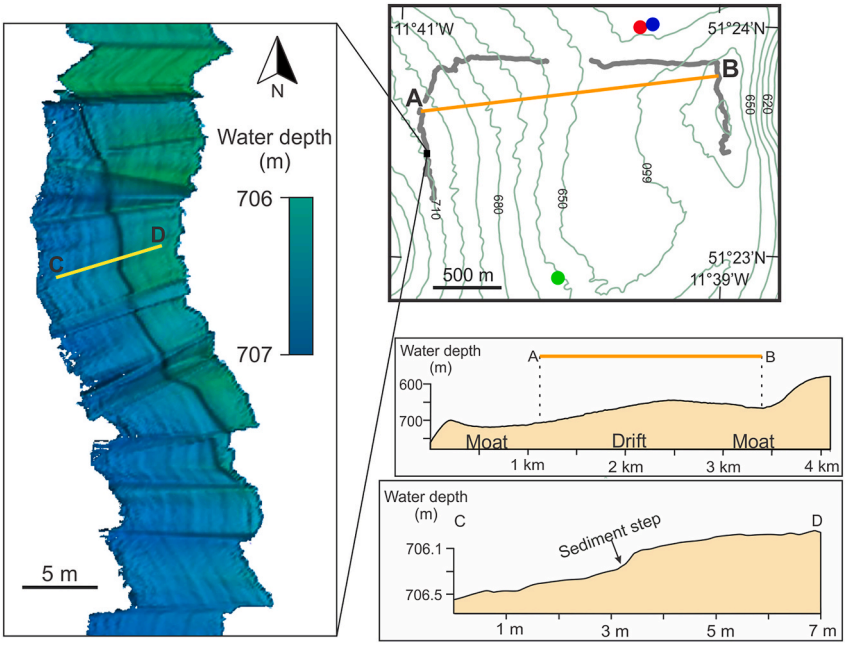

Fig. 4. Bathymetric cross-section profile over the Belgica Mound Drift (A-B orange line), based on the 2022 bathymetric data (Fig. 1), and a small profile within the western moat (C-D yellow line), based on the 2019 ROV-acquired bathymetry. Given the presence of numerous along-track artefacts, only across-track height differences are considered. The mooring sites are represented by red (2021-M1), blue (2019-M1) and green (2021-M2) dots. The grey line corresponds to the ROV track. (For interpretation of the references to colour in this figure legend, the reader is referred to the Web version of this article.)

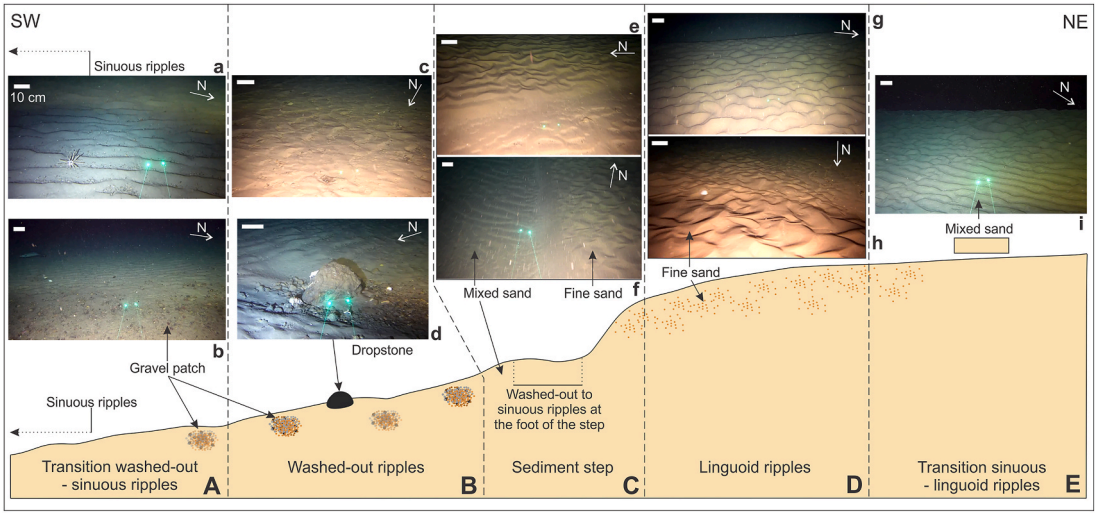

Fig. 5. Schematic illustration (not to scale) of the observed ripple sequence on the western track, featuring images from the ROV dive. A 10 cm scale reference is shown by the white bar in the top left corner of each screenshot. The distance scale is only valid for the center of the image. Screenshots of the video frames were extracted for illustrative purpose. The locations of the screenshots (indicated by lowercase letters) are shown on Fig. 6.

Table 3
Range of the dimensions of the different encountered bedforms.

Scale	Bedform	Wavelength *(crest to crest distance)*	Height/Amplitude *(trough to crest height)*
Small-scale	Straight to sinuous ripples	5–20 cm	2–5 cm
	Linguoid ripples	5–25 cm	2–5 cm
	Washed-out ripples	5–20 cm	>1 cm
Large-scale	Sediment steps	10–50 m (western moat) 10 m (eastern moat)	10–40 cm

been observed along the ROV track: 13 in the eastern moat and 17 in the western moat, occurring between 658 and 712 m water depth. The ROV followed one sediment step for 150 m in the western moat (Fig. 6b), showing a rather straight crest line over the entire track. Washed-out ripples and linguoid ripples are more common in the western moat and sinuous ripples more often observed on the crest of the drift and in the eastern moat. Dropstones are commonly observed in the areas with the washed-out ripples (Fig. 6a, 6c) and on the crest of the drift (Fig. 6d).

5. Discussion

5.1. Present-day temporal variability of bottom currents

The measured bottom current strength and direction (Fig. 3; Table 2) concur with what has been previously observed in the Belgica Mound Province through other direct measurements (White et al., 2007; Dorschel et al., 2007): The bottom currents are dominated by an intensified across-slope (W–E, SW–NE) diurnal tidal component with a weaker northward (alongslope) residual component. Measurements reported here are unique since, for the first time, several moorings yielded spatial and temporal information about the hydrodynamic regime over a relatively small contourite drift.

Both the 2021 moorings were affected by suspected trawling activity, resulting in the loss of near-seabed current meters. Only the current meters positioned at 35 m above the seafloor remained, reducing data completeness and limiting full comparison with the 2019 dataset. Additionally, differences in deployment year and recording period further limit the comparison between locations. Minor differences between the 2021 mooring data are likely due to the small-scale topographic variabilities in the vicinity of the measurements. The velocity readings for both current meters at 35 m above the seafloor in the north and south of the drift crest are similar (Table 2) and show weaker bottom currents than at 6 m above the seafloor (Fig. 3A). It is known that the bottom currents, mostly driven by trapped diurnal baroclinic waves, are enhanced near the seafloor within the northern section of the Belgica Mound Province (White, 2007). A weaker steering effect of the currents at 35 m, being further away from the local topography, i.e. CWC mounds and the drift topography, may be the reason for their W–E component, rather than the SW–NE orientation at 6 m above the seafloor (Fig. 3A). In other words, the closer to the seafloor, the more the currents show interaction with the variable seafloor topography. Consequently, the 2019-M1 data, collected at 6 m above the seafloor, would be more representative of the hydrodynamic regime on the drift, responsible for the formation of the bedforms, compared to the 2021 mooring data collected at 35 m above the seafloor.

This also suggests that the diurnal tidal components are amplified as found by White et al. (2007) and small-scale spatial variability is comparable to other locations within the Belgica Mound Province (Dorschel et al., 2007). The measured residual northward current combines both the alongslope bottom current generated by the trapped baroclinic motion (Huthnance, 1981; White and Dorschel, 2010) and the bottom current related to the European Slope Current (thermohaline circulation; Toucanne et al., 2021).

The observed asymmetry in temperature fluctuations (Fig. 3C) further supports the presence of the trapped tidal baroclinic motion and its interaction with the topography. Specifically, the sharp temperature drops during the shorter upslope flow contrasts with the more gradual increases during the longer downslope flow. The upslope flows (towards E for 2021 moorings or NE for 2019-M1) exhibit higher velocities than the downslope flows (Fig. 3C). This pattern is associated with the movement of colder and deeper water during upslope flow. This has been often observed for freely propagating baroclinic motion on slopes (e.g. White, 1994; Lorke et al., 2005) and also for diurnal tidal motions on the slopes of the Rockall Bank (Mienis et al., 2007)0.5.2 Sediment steps: dunes or waves?

One should be aware that the ROV visual imagery only represents a “snapshot” of the seabed morphology, displaying the seafloor features at the time of data collection. The presented dataset does not allow for the interpretation of the bedforms in terms of temporal variability. Since diurnal tidal currents are active in the area, acquisition of visual data 6 h sooner or later could result in different sizes and/or orientations of the

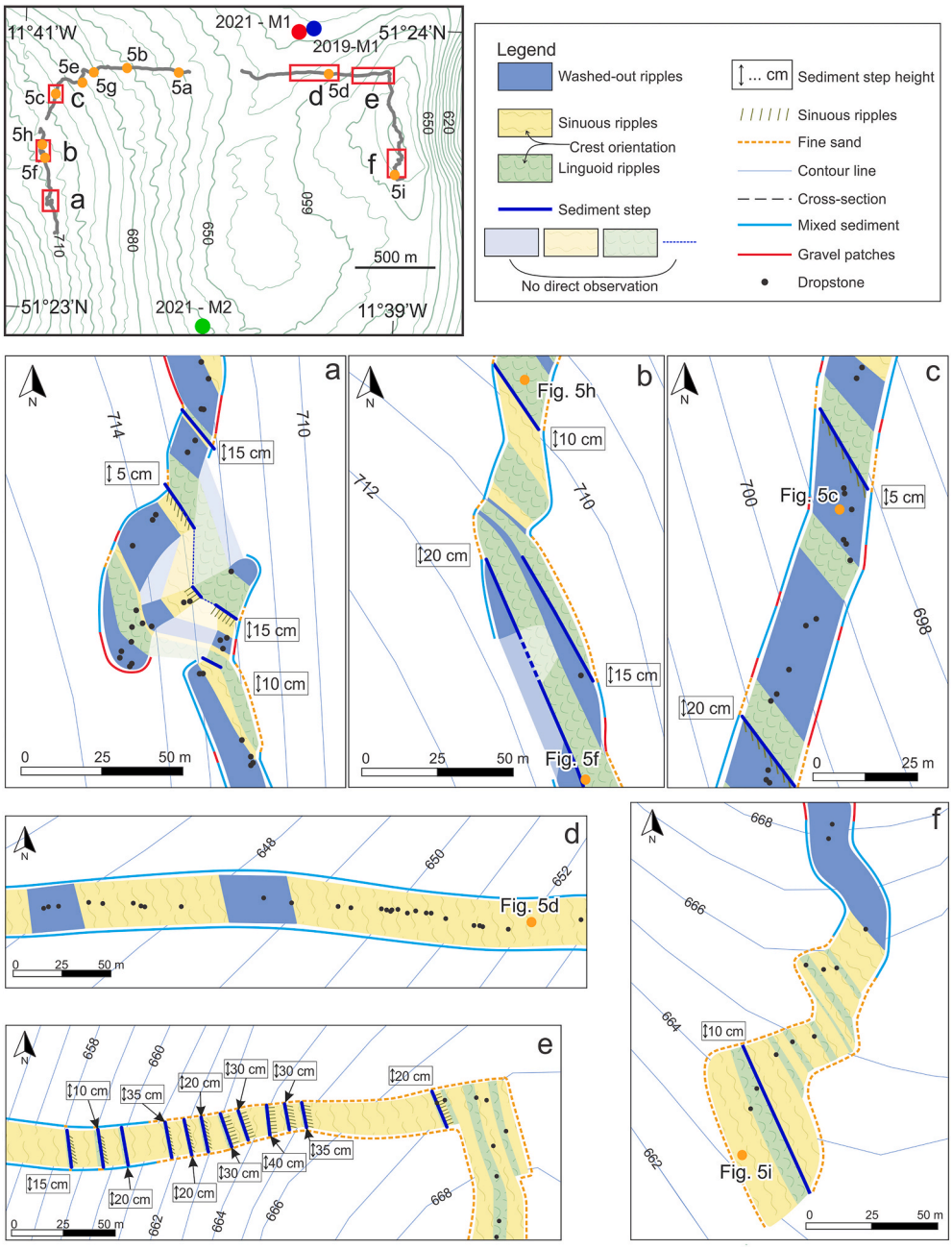

Fig. 6. Sediment bedform maps (a to f, location see top left panel) including various features observed using the ROV HD video data. The locations of the screenshots shown in Fig. 5 are marked by orange dots. (For interpretation of the references to colour in this figure legend, the reader is referred to the Web version of this article.)

observed bedforms. It is assumed these are mobile bedforms, which is difficult to assess from this present dataset.

The large-scale features described as sediment steps (Figs. 5 and 6) could correspond to two types of features based on their size (height differences up to 40 cm high), shape and distance between two features (between 10 and 50 m).

A similar ripple succession superimposed on larger scale features (crest height between 0.3 and 0.9 m and wavelengths of 3.5–5 m) was described by Stow et al. (2013) within the Cadiz Contourite Channel. According to their interpretation, the large-scale bedforms could be sinuous to crescent sediment waves and dunes, both with asymmetrical smaller-scale ripples on the stoss side (upstream) and a smooth lee side (downstream). Wynn et al. (2002) and Jiménez-Romero et al. (2022) also presented a similar sequence of ripples on top of, respectively, barchan dunes (crest height >50 cm and 10–30 m wavelengths) and dunes. Barchan dunes have already been described in the Belgica Mound Province, NW of the study area (Wheeler et al., 2005). However, all observed sediment steps display a straight crest (Fig. 6), can at least be 150 m long and do not have a distinct dune shape.

A multitude of similar seabed features were also observed near the CWC mounds in the Belgica Mound Province through high-resolution side-scan sonar (Wheeler et al., 2005; Huvenne et al., 2005) and ROV imagery (Foubert et al., 2005). Here, the seafloor is typically made up of rippled sand with superimposed smaller-scale ripples on top of sediment waves (Foubert et al., 2005; Wheeler et al., 2005; Huvenne et al., 2005). These sediment waves were observed mainly in the vicinity of the Moira Mounds (NW of study area; Fig. 1). They are described as straight, long-crested (several hundreds of metres long), asymmetric, up to 50 cm

high and with wavelengths of 15–20 m. Superimposed smaller-scale straight to linguoid ripples were also observed on top of those larger-scale bedforms (Foubert et al., 2005, 2011). The dimensions and shape of these features correspond to the described sediment steps (Figs. 5 and 6), however, their lengths differ. The longest sediment step crest observed with the ROV was 150 m long and is possibly even longer.

Taking into account the description and interpretation made by Foubert et al. (2005, 2011), it is most likely the observed sediment steps can be interpreted as sediment waves. A deep-water sediment wave is defined as a large-scale depositional bedform generated by bottom currents (Wynn et al., 2000). These features usually have wavelengths of tens of metres to a few kilometres and a height of several metres. Therefore, the observed features could be interpreted as small-scale sediment waves with superimposed ripples. The main deviation from the definition is that the described sediment steps have steep, nearly vertical, lee sides (Figs. 4 and 5) which may be due to erosional processes rather than strictly depositional processes. The straight to sinuous parallel to perpendicular ripples visible at the foot of the sediment waves (Fig. 5C) could be interference ripples, also known as ladderback ripples (Ramsay et al., 1989). Similar ripples (average wavelength of 7.7 cm and crest height of 1 cm) have been observed by Jiménez-Romero et al. (2022) in the trough of dunes on the Gulf of Cadiz. These ripples are often due to the refraction of oblique waves in coastal areas and highlight the presence of two current directions, either occurring simultaneously or successively (Ramsay et al., 1989). Although their origin in deeper environments is still not well understood (Jiménez-Romero et al., 2022), Stow et al. (2013) linked them to tidal currents, as observed in the area through the mooring data. The lee side of the sediment waves (Figs. 4 and 5) could form an obstacle to the primary flow, i.e. the across-slope tidal current measured with the moorings. The lee side would modify the current speed and direction by refracting the current towards the NW (Fig. 7). This secondary refracted flow has the ability to erode the lee side of the sediment waves, changing the shape of the sediment waves and making their lee side almost vertical. The secondary flow can also trigger the formation of straight to sinuous ripples at the foot of the sediment wave, with their crest oblique or even perpendicular to the crest orientation of the sediment wave (Fig. 5). The northward refracted flow could consequently play a role in the erosion of the lee side of the sediment waves and the local formation of small-scale bedforms.

5.2. Deduced bottom-current velocity and direction

Hydrodynamic processes are at work in the study area, as evidenced by the absence of degradation of the observed bedforms or the absence of bioturbations over the small-scale bedforms (Fig. 5). This either demonstrates that the bedforms are very recently formed or still actively developing. The observed bedforms can thus be used to assess the present-day hydrodynamic regime over the drift and be compared with the mooring data.

As both sediment waves and their superimposed ripples have the same crest orientation, it is reasoned that both are related to the same hydrodynamic processes. The alignment of the small-scale ripples and the sediment waves, with their NNW–SSE crests, indicates an across-slope flow direction perpendicular to the moats and drift orientation. On the eastern side of the drift crest, the inferred flow direction is towards ENE while on the western side, the flow direction is towards WSW (Fig. 7). These directions are consistent with the mooring observations and the direction of the across-slope tidal current. The residual along-slope northward current seems to have no direct influence on the bedform formation as no perpendicular ripples have been observed.

Flow velocities can be derived by examining the type of ripples, coupled with the seafloor texture, and using the matrix of Stow et al. (2009) (Table 4; Fig. 7). This matrix describes the flow velocities and the grain size needed to form different type of ripples. The grain size likely corresponds to coarse sand (Huvenne et al., 2005; Van Rooij et al., 2007) and is approximately 0.1 mm. The model of Stow et al. (2009) is an approximation, as the development of bedforms depends on several other physical parameters that were not taken into account in this interpretation, such as the fluid density, particle density, and sediment supply (Stow et al., 2009). The exact value of the flow responsible for a given type of bedform is difficult to evaluate, but the range of involved flow velocities can still be estimated using this model.

The across-slope tidal current, flowing up to 50 cm/s in a W or E direction as evidenced by the 2019-M1 mooring data (Fig. 3; Table 2), is strong enough to induce the sinuous and linguoid ripples (Table 4). The asymmetry of these ripples highlights their formation under one dominant flow direction. They could be created every tidal episode and the few bioturbations observed in association with the straight to sinuous ripples could be formed and eroded after each tidal passing.

Table 4
Inferred flow velocities based on the ripple type. The washed-out ripples are not included in the Stow et al. (2009) bedform matrix. Baas and De Koning (1995) made an experiment with a grain size of 0.108 mm.

Ripple type	Inferred velocity range	Reference
Straight to sinuous	10–20 cm/s	Stow et al. (2009)
Linguoid	30–50 cm/s	Stow et al. (2009)
Washed-out	75–91 cm/s	Baas and De Koning (1995)
Sediment waves	75–100 cm/s	Huvenne et al. (2005)
	50–120 cm/s	Soulsby (1997)

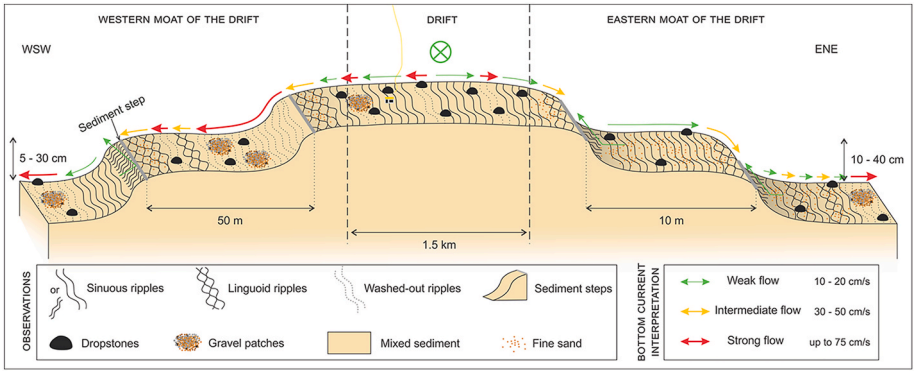

Fig. 7. 3D sketch of an idealised cross-section profile (not to scale) over the crest and the western and eastern moats of the Belgica Mound Drift (northern sector). This shows the succession of the observed bedforms as well as the inferred current velocities and directions. The green arrows correspond to a weaker flow (10–20 cm/s), orange arrows to an intermediate flow (30–50 cm/s) and red arrows to a stronger flow (up to 75 cm/s). The circled cross indicates the alongslope residual current directed into the plane of the figure. (For interpretation of the references to colour in this figure legend, the reader is referred to the Web version of this article.)

Consequently, they only indicate the direction of the last tidal flow that has passed in the area. The straight to sinuous ripples are representative of the present-day hydrodynamic regime, in term of bottom-current velocities and directions, that are also recorded by the mooring data.

The origin of the washed-out ripples and the sediment waves (Table 4) cannot be explained solely by the flow velocities measured in the area (Fig. 3; Table 2; Pingree and Le Cann, 1990; Rice et al., 1991; White, 2007; Dorschel et al., 2009) as present currents are not stronger than 50 cm/s. Huvenne et al. (2005), Wheeler et al. (2005) and Foubert et al. (2011) mentioned that the large-scale features in the vicinity of the Moira Mounds may be related to not yet recorded peak flow events. Similarly, the sediment waves could not be shaped by the average diurnal tidal flow and could instead be related to peak flow events. As such, the sediment waves could be relict features formed by strong bottom currents occurring at any time since the last glacial period, possibly associated with a recent unrecorded peak flow event. The reintroduction of the MOW in a post-glacial Porcupine Seabight could be responsible for an amplification of the bottom current strength and a transition into an environment with higher sediment mobilisation at the beginning of the current interglacial period (Huvenne et al., 2009; Raddatz et al., 2011). To better understand the processes responsible for the formation and mobilisation of these large-scale features, a more detailed investigation of the seafloor is required. In particular, confirming the identification of the sediment waves depends on accurately determining their dimensions. Without this information, it remains difficult to confirm their origin and evaluate the hydrodynamic conditions under which they formed.

The wide variety of bedforms observed on the crest and within the moats of the drift indicates important spatial variations of the bottom-current velocity (Fig. 7), sometimes over a few metres (Fig. 6). The NNW–SSE orientation of the boundaries between the bedform areas, which is parallel to slightly oblique to the bathymetric contours, reflects the importance of the local topography in the formation of these bedforms. The spatial variation of ripple patterns highlights the flow variation over the drift, with increased flow velocities on the drift moats enabling the daily formation of linguoid ripples (Fig. 7). The crest of the drift, even if no linguoid ripples have been observed there (Figs. 6 and 7), is still under a dynamic regime allowing the formation of straight to sinuous ripples and even washed-out ripples during more intense hydrodynamic events. It is possible that the peak flow events were significantly more intense in the moats than over the drift, as the sediment waves are exclusively seen in the moats (Figs. 6 and 7). During these post-last glacial peak events, the local topography, such as the drift and moat geometry and the CWC mounds, played a crucial role in local enhancement of the across-slope currents in the moats. While the drift was formed under the influence of an alongslope current since the Early Pleistocene (Matossian and Van Rooij, 2024), it is not presently the dominant current component influencing the drift and the moats. Indeed, nowadays, the across-slope tidal current plays a bigger role than the residual northward (alongslope) current. Numerous dropstones have also been observed by Huvenne et al. (2005), Foubert et al. (2005) and Wheeler et al. (2005) near the Moira Mounds. The presence of dropstones, with scours upstream and gravel patches downstream, confirms at least the occurrence of a post-last glacial highly dynamic flow regime eroding the seafloor in the Belgica Mound Province (Foubert et al., 2005; Huvenne et al., 2005; Wheeler et al., 2005) and a low sediment input in the present-day, preventing the moats to be filled in and the dropstones to be buried.

6. Conclusions

This work, focusing on the small-scale Belgica Mound Drift, has shown that bedforms, moorings and detailed analysis of ROV imagery yields valuable insights into the present-day hydrodynamic regime and its influence on the spatial and temporal drift evolution.

While the contourite drift was formed under persistent alongslope bottom currents since the Early Pleistocene (Matossian and Van Rooij, 2024), the present-day main flow directions are perpendicular to the drift crest, showing that the main oceanographic processes responsible for the formation of the drift are currently not playing a role in the evolution of the drift. Nevertheless, the Belgica Mound Drift and mostly its moats are still affected by a strong hydrodynamic regime, with depositional and erosional processes. The observed currents are enhanced closer to the seafloor, with recorded speeds up to 50 cm/s, whereas the velocities inferred from the bedforms range from 10 to 100 cm/s. The lowest inferred velocities are related to the recorded diurnal tidal flows and the highest linked to not yet recorded peak flow events, responsible for the formation of sediment waves. Defining the full extension of these sediment waves, which is still unknown from the ROV imagery, could give a better idea about the processes involved in their formation.

At a closer scale, the spatial variability of the bottom-current velocities is demonstrated by the spatial distribution of the bedforms that varies over a few metres. This is related to the local topography, such as the CWC mounds, the drift topography and the sediment waves deflecting and steering the bottom currents. As a result, the large-scale bedforms affect locally the bottom flows and the formation of small-scale ripples.

The hydrodynamic analysis relies on limited statistical treatment due to data loss and differences in deployment year and recording period, which constrain comparison between datasets. Additionally, this study does not include quantitative morphological reconstructions from ROV imagery, such as could be achieved through photogrammetry. However, the integrated approach still provides valuable insights. These limitations highlight opportunities for future research to build upon this foundation using more advanced methods. Although the conclusions are specific to the Belgica Mound Drift, the methodologies applied here can serve as a useful framework for investigating similar contourite systems in other deep-water environments.

Therefore, the identification of bedforms through the ROV imagery, in complement with mooring data, is an efficient method to investigate the spatial variations of the bottom currents in a deep environment and allows to comprehend their dynamic influence on the construction of a contourite drift.

CRediT authorship contribution statement

Alice O. Matossian: Writing – review & editing, Writing – original draft, Visualization, Investigation, Formal analysis. **Eoghan Daly:** Writing – review & editing, Data curation. **Sheena Fennell:** Writing – review & editing, Data curation. **Nadzeya Shymbaliova:** Investigation. **Thomas Vandorpe:** Writing – review & editing, Supervision, Resources, Methodology, Formal analysis, Data curation. **Martin White:** Writing – review & editing, Writing – original draft, Supervision, Resources, Methodology, Investigation, Data curation. **David Van Rooij:** Writing – review & editing, Supervision, Project administration, Investigation, Funding acquisition, Conceptualization.

Declaration of competing interest

The authors declare that they have no known competing financial interests or personal relationships that could have appeared to influence the work reported in this paper.

Acknowledgements

This research was conducted in the framework of the FWO project “DynaMOD” (FWO grant 3G021719) and on the BOF extension BOF23/CDV/126. Ship time on RV Belgica was provided by BELSPO and RBINS-OD Nature. This study uses ROV Zonnebloem (previously ROV Genesis) provided by Flanders Marine Institute. We would like to thank Willem Versteeg and Robin Houthoofdt for their help with the ROV during the

RV Belgica 2019/16 survey. The deployment of the 2021 moorings was kindly facilitated by the Marine Institute (Ireland) during the CE21014 weather buoy maintenance survey. We kindly acknowledge the two anonymous reviewers for their comments which improved the quality of this manuscript.

Data availability

Data from campaign Belgica 2019/17 is part of ongoing research and is not yet available in any repository.

References

Baas, J.H., De Koning, H., 1995. Washed-out ripples: their equilibrium dimensions, migration rate, and relation to suspended-sediment concentration in very fine sand. J. Sediment. Res. 65, 431–435. https://doi.org/10.1306/D42680E5-2B26-11D7-8648000102C1865D.

Baines, P.G., 1974. The generation of internal tides over steep continental slopes. Philos. Trans. R. Soc. Lond., Ser. A Math. Phys. Sci. 277, 27–58. https://doi.org/10.1098/rsta.1974.0045.

Besio, G., Blondeaux, P., Brocchini, M., Vittori, G., 2003. Migrating sand waves. Ocean Dyn. 53, 232–238. https://doi.org/10.1007/s10236-003-0043-x.

Boyer, T.P., Baranova, O.K., Coleman, C., García, H.E., Grodsky, A., Locarnini, R.A., Mishonov, A.V., Paver, C.R., Reagan, J.R., Seidov, D., Smolyar, I.V., Weathers, K.W., Zweng, M.M., 2018. In: Mishonov, A.V., Technical (Eds.), World Ocean Database 2018, 87. NOAA Atlas NESDIS.

Chachkine, P., Akhmetzhanov, A.M., 1998. Subbottom currents on the porcupine margin study by side-scan sonars. In: De Mol, B. (Ed.), Geosphere-Biosphere Coupling: Carbonate Mud Mounds and Cold Water Reefs, 143. UNESCO, Paris, p. 30. IOC Workshop Report.

Dorschel, B., Hebbeln, D., Foubert, A., White, M., Wheeler, A.J., 2007. Hydrodynamics and cold-water coral facies distribution related to recent sedimentary processes at Galway mound west of Ireland. Mar. Geol. 244, 184–195. https://doi.org/10.1016/j.margeo.2007.06.010.

Dorschel, B., Wheeler, A.J., Huvenne, V.A.I., de Haas, H., 2009. Cold-water coral mounds in an erosive environmental setting: TOBI side-scan sonar data and ROV video footage from the northwest Porcupine Bank, NE Atlantic. Mar. Geol. 264, 218–229. https://doi.org/10.1016/j.margeo.2009.06.005.

Foubert, A., Beck, T., Wheeler, A.J., Opderbecke, J., Grehan, J., Klages, M., Thiede, J., Henriet, J.-P., Polarstern ARK-XIX/3a Shipboard Party, 2005. New view of the Belgica Mounds, Porcupine Seabight, NE Atlantic: preliminary Results from the Polarstern ARK-XIX/3a ROV cruise. In: Freiwald, A., Roberts, J.M. (Eds.), Cold-Water Corals and Ecosystems. Springer, Heidelberg, pp. 403–415. https://doi.org/10.1007/3-540-27673-4_20.

Foubert, A., Huvenne, V.A.I., Wheeler, A.J., Kozachenko, M., Opderbecke, J., Henriet, J.-P., 2011. The Moira Mounds, small cold-water coral mounds in the Porcupine Seabight, NE Atlantic: part B—evaluating the impact of sediment dynamics through high-resolution ROV-borne bathymetric mapping. Mar. Geol. 282, 65–78. https://doi.org/10.1016/j.margeo.2011.02.008.

Hanquiez, V., Mulder, T., Lecroart, P., Gonthier, E., Marchès, E., Voisset, M., 2007. High resolution seafloor images in the Gulf of Cadiz, Iberian margin. Mar. Geol. 246, 42–59. https://doi.org/10.1016/j.margeo.2007.08.002.

Harvey, J., 1982. θ-S relationships and water masses in the eastern North Atlantic. deep-sea. Res. I: Oceanogr. Res. Pap. 29, 1021–1033. https://doi.org/10.1016/0198-0149(82)90025-5.

Hollister, C.D., Heezen, B.C., 1972. Geologic effects of ocean bottom currents. In: Gordon, A.L. (Ed.), Studies in Physical Oceanography, 2. Gordon and Breach, New York, pp. 37–66.

Huthnance, J.M., 1981. Waves and currents near the continental shelf edge. Prog. Oceanogr. 10, 193–226. https://doi.org/10.1016/0079-6611(81)90004-5.

Huvenne, V., Beyer, A., de Haas, H., Dekindt, K., Henriet, J.-P., Kozachenko, M., Olu-Le Roy, K., Wheeler, A.J., TOBI/Pelagia 197, CARACOLE cruise participants, 2005. The seabed appearance of different coral bank provinces in the Porcupine Seabight, NE Atlantic: results from sidescan sonar and ROV seabed mapping. In: Freiwald, A., Roberts, J.M. (Eds.), Cold-Water Corals and Ecosystems. Springer, Heidelberg, pp. 535–569.

Huvenne, V.A.I., Van Rooij, D., De Mol, B., Thierens, M., O'Donnell, R., Foubert, A., 2009. Sediment dynamics and palaeo-environmental context at key stages in the challenger cold-water coral mound formation: clues from sediment deposits at the mound base. Deep-Sea Res. I Oceanogr. Res. Pap. 56, 2263–2280. https://doi.org/10.1016/j.dsr.2009.08.003.

INFOMAR, 2023. INFOMAR Marine Data Download Portal [WWW Document].

Iorga, M.C., Lozier, M.S., 1999. Signatures of the Mediterranean outflow from a North Atlantic climatology: 2. Diagnostic velocity fields. J. Geophys. Res. Oceans 104, 26011–26029. https://doi.org/10.1029/1999JC900204.

Jiménez-Romero, R., Fernandez-Salas, L.M., Palomino, D., Sanchez-Leal, R.F., Vila, Y., 2022. Discovering the fine-scale morphology of the Gulf of Cádiz: an underwater imaging analysis. J. Mar. Sci. Eng. 10, 651. https://doi.org/10.3390/jmse10050651.

Kenyon, N.H., Belderson, R.H., 1973. Bedforms of the Mediterranean undercurrent observed with sidescan sonar. Sediment. Geol. 9, 77–99. https://doi.org/10.1016/0037-0738(73)90027-4.

Kenyon, N.H., Ivanov, M.K., Akhmetzhanov, A.M., 1998. Cold water carbonate mounds and sediment transport on the north-east Atlantic margin. In: IOC Tech Ser, 52. UNESCO, Paris.

Khélifi, N., Sarnthein, M., Andersen, N., Blanz, T., Frank, M., Garbe-Schönberg, D., Haley, B.A., Stumpf, R., Weinelt, M., 2009. A major and long-term Pliocene intensification of the Mediterranean outflow, 3.5-3.3 Ma ago. Geology 37, 811–814. https://doi.org/10.1130/G30058A.1.

Khélifi, N., Sarnthein, M., Frank, M., Andersen, N., Garbe-Schönberg, D., 2014. Late Pliocene variations of the Mediterranean outflow. Mar. Geol. 357, 182–194. https://doi.org/10.1016/j.margeo.2014.07.006.

Lo Iacono, C., Guillen, J., Guerrero, Q., Duran, R., Wardell, C., Hall, R.A., Aslam, T., Carter, G.D.O., Gales, J.A., Huvenne, V.A.I., 2020. Bidirectional bedform fields at the head of a submarine canyon (NE Atlantic). Earth Planet Sci. Lett. 542, 116321. https://doi.org/10.1016/j.epsl.2020.116321.

Lorke, A., Peeters, F., Wüest, A., 2005. Shear-induced convective mixing in bottom boundary layers on slopes. Limnol. Oceanogr. 50, 1612–1619. https://doi.org/10.4319/lo.2005.50.5.1612.

Masson, D.G., Wynn, R.B., Bett, B.J., 2004. Sedimentary environment of the Faroe-Shetland channel and Faroe Bank channels, NE Atlantic, and the use of bedforms as indicators of bottom current velocity in the deep ocean. Sedimentology 51, 1–35. http://doi.org/10.1111/j.1365-3091.2004.00668.x.

Marine Institute, 2019. Marine data centre, tidal observations [online]. Available at: https://data.marine.ie/. June 2019.

Matossian, A.O., Van Rooij, D., 2024. Morphosedimentary evolution of the Belgica Mound drift: controls on contourite depositional system development in association with cold-water coral mounds. Mar. Geol. 477, 107410. https://doi.org/10.1016/j.margeo.2024.107410.

McCartney, M., Mauritzen, C., 2001. On the origin of the warm inflow to the Nordic seas. Prog. Oceanogr. 51, 125–214. https://doi.org/10.1016/S0079-6611(01)00084-2.

McDonnell, A., Shannon, P.M., 2001. Comparative tertiary stratigraphic evolution of the Porcupine and Rockall basins. Geol. Soc. London Spec. Publ. 188, 323–344. https://doi.org/10.1144/GSL.SP.2001.188.01.19.

Mienis, F., De Stigter, H.C., White, M., Duineveld, G., De Haas, H., Van Weering, T.C.E., 2007. Hydrodynamic controls on cold-water coral growth and carbonate-mound development at the SW and SE Rockall trough margin, NE Atlantic Ocean. Deep-Sea Res. I Oceanogr. Res. Pap. 54, 1655–1674. https://doi.org/10.1016/j.dsr.2007.05.013.

Mulder, T., Voisset, M., Lecroart, P., Le Drezen, E., Gonthier, E., Hanquiez, V., Faugères, J.C., Habgood, E., Hernández-Molina, F.J., Estrada, F., Llave-Barranco, E., Poirier, D., Gorini, C., Fuchey, Y., Voelker, A., Freitas, P., Lobo, S.F., Fernandez, L. M., Kenyon, N.H., Morel, J., 2003. The Gulf of Cadiz: an unstable giant contouritic levee. Geo Mar. Lett. 23, 7–18. https://doi.org/10.1007/s00367-003-0119-0.

Naylor, D., Shannon, P.M., 1982. Geology of Offshore Ireland and West Britain, 1982 edition. Springer, London.

Nelson, C.H., Baraza, J., Maldonado, A., 1993. Mediterranean under current sandy contourites, Gulf of Cadiz, Spain. Sediment. Geol. 82, 103–131. https://doi.org/10.1016/0037–0738(93)90116-M.

New, A.L., Barnard, S., Herrmann, P., Molines, J.-M., 2001. On the origin and pathway of the saline inflow to the Nordic seas: insights from models. Prog. Oceanogr. 48, 255–287. https://doi.org/10.1016/S0079-6611(01)00007-6.

Pearson, I., Jenkins, D.G., 1986. Unconformities in the Cenozoic of the North-East Atlantic. In: Summerhayes, C.P., Shackleton, N.J. (Eds.), North Atlantic Palaeoceanography. Soc. London Spec. Publ, Geol, pp. 79–86.

Pingree, R.D., Le Cann, B., 1989. Celtic and Armorican slope and shelf residual currents. Prog. Oceanogr. 23, 303–338. https://doi.org/10.1016/0079-6611(89)90003-7.

Pingree, R.D., Le Cann, B., 1990. Structure, strength and seasonality of the slope currents in the Bay of Biscay region. J. Mar. Biol. Assoc. U. K. 70, 857–885. https://doi.org/10.1017/S0025315400059117.

Raddatz, J., Rüggeberg, A., Margreth, S., Dullo, W.-C., 2011. Paleoenvironmental reconstruction of challenger mound initiation in the Porcupine Seabight, NE Atlantic. Mar. Geol. 282, 79–90. https://doi.org/10.1016/j.margeo.2010.10.019.

Ramsay, P.J.C., Cooper, A., Wright, C.I., Mason, T.R., 1989. The occurrence and formation of ladderback ripples in subtidal, shallow-marine sands, Zululand, South Africa. Mar. Geol. 86, 229–235.

Rebesco, M., Hernández-Molina, F.J., Van Rooij, D., Wåhlin, A., 2014. Contourites and associated sediments controlled by deep-water circulation processes: state-of-the-art and future considerations. Mar. Geol. 352, 111–154. https://doi.org/10.1016/j.margeo.2014.03.011.

Rice, A.L., Billett, D.S.M., Thurston, M.H., Lampitt, R.S., 1991. The institute of oceanographic sciences biology programme in the Porcupine Seabight: background and general introduction. J. Mar. Biol. Assoc. U. K. 71, 281–310. https://doi.org/10.1017/S0025315400051614.

Schlitzer, R., 2021. Ocean data view [online]. Available at: https://odv.awi.de. October 2021.

Simons, D.B., Richardson, E.V., 1966. Resistance to flow in alluvial channels. J. Hydraul. Eng. 86, 73–99. https://doi.org/10.3133/pp422J.

Soulsby, R.L., 1997. Dynamics of Marine Sands: a Manual for Practical Applications. Thomas Telford, London.

Stow, D.A.V., 1982. Bottom currents and contourites in the North Atlantic. Bull. Inst. Geol. Bassin Aquitaine 31, 151–166.

Stow, D.A.V., Hernández-Molina, F.J., Llave, E., Sayago-Gil, M., Diaz del Rio, V., Branson, A., 2009. Bedform-velocity matrix: the estimation of bottom current velocity from bedform observations. Geology 37, 327–330. https://doi.org/10.1130/G25259A.1.

Stow, D.A.V., Hernández-Molina, F.J., Llave, E., Bruno, M., García, M., Díaz del Rio, V., Somoza, L., Brackenridge, R.E., 2013. The Cadiz Contourite channel: sandy

contourites, bedforms and dynamic current interaction. Mar. Geol. 343, 99–114. https://doi.org/10.1016/j.margeo.2013.06.013.
Toucanne, S., Soulet, G., Riveiros, N.V., Boswell, S.M., Dennielou, B., Waelbroeck, C., Bayon, G., Mojtahid, M., Bosq, M., Sabine, M., Zaragosi, S., Bourillet, J.-F., Mercier, H., 2021. The North Atlantic glacial eastern boundary current as a key driver for ice-sheet—Amoc interactions and climate instability. Paleoceanogr. Paleoclimatol. 36. https://doi.org/10.1029/2020PA004068.
Tucholke, B.E., Hollister, C.D., Biscaye, P., Gardner, W., 1985. Abyssal current character determined from sediment bedforms on the Nova Scotian continental rise. Mar. Geol. 66, 43–58. https://doi.org/10.1016/0025-3227(85)90022-2.
van Aken, H.M., Becker, G., 1996. Hydrography and through-flow in the north-eastern North Atlantic Ocean: the NANSEN project. Prog. Oceanogr. 38, 297–346. https://doi.org/10.1016/S0079-6611(97)00005-0.
van Aken, H.M., 2000. The hydrography of the mid-latitude Northeast Atlantic Ocean: II: the intermediate water masses. Deep-Sea Res. I Oceanogr. Res. Pap. 47, 789–824. https://doi.org/10.1016/S0967-0637(99)00112-0.
Van Rooij, D., De Mol, B., Huvenne, V., Ivanov, M., Henriet, J.-P., 2003. Seismic evidence of current-controlled sedimentation in the Belgica mound province, upper Porcupine slope, southwest of Ireland. Mar. Geol. 195, 31–53. https://doi.org/10.1016/S00253227(02)00681-3.
Van Rooij, D., Blamart, D., Kozachenko, M., Henriet, J.-P., 2007. Small mounded contourite drifts associated with deep-water coral banks, Porcupine Seabight, NE Atlantic Ocean. Geol. Soc. Lond. Spec. Publ. 276, 225–244. https://doi.org/10.1144/GSL.SP.2007.276.01.11.
Van Rooij, D., Huvenne, V.A.I., Blamart, D., Henriet, J.-P., Wheeler, A., de Haas, H., 2009. The Enya mounds: a lost mound-drift competition. Int. J. Earth Sci. 98, 849–863. https://doi.org/10.1007/s00531-007-0293-9.
Wheeler, A.J., Bett, B.J., Billet, D.S.M., Masson, D.G., 2000. Very high resolution side-scan mapping of deep-water coral mounds: surface morphology and processes affecting growth. EOS Trans. 81, 48.
Wheeler, A.J., Kozachenko, M., Beyer, A., Foubert, A., Huvenne, V.A.I., Klages, M., Masson, D.G., Olu-Le Roy, K., Thiede, J., 2005. Sedimentary processes and carbonate mounds in the Belgica Mound province, Porcupine Seabight, NE Atlantic. In: Freiwald, A., Roberts, J.M. (Eds.), Cold-Water Corals and Ecosystems. Springer, Heidelberg, pp. 571–603. https://doi.org/10.1007/3-540-27673-4_28.
White, M., 1994. Tidal and subtidal variability in the sloping benthic boundary layer. J. Geophys. Res. Oceans 99, 7851–7864. https://doi.org/10.1029/93JC03211.
White, M., 2007. Benthic dynamics at the carbonate mound regions of the Porcupine Sea Bight continental margin. Int. J. Earth Sci. 96, 1–9. https://doi.org/10.1007/s00531-006-0099-1.
White, M., Roberts, J.M., van Weering, T., 2007. Do bottom-intensified diurnal tidal currents shape the alignment of carbonate mounds in the NE Atlantic? Geo Mar. Lett. 27, 391–397. https://doi.org/10.1007/s00367-007-0060-8.
White, M., Dorschel, B., 2010. The importance of the permanent thermocline to the cold water coral carbonate mound distribution in the NE Atlantic. Earth Planet Sci. Lett. 296, 395–402. https://doi.org/10.1016/j.epsl.2010.05.025.
Wynn, R.B., Weaver, P.P.E., Ercilla, G., Stow, D.A.V., Masson, D.G., 2000. Sedimentary processes in the Selvage sediment-wave field, NE Atlantic: new insights into the formation of sediment waves by turbidity currents. Sedimentology 47, 1181–1197.
Wynn, R.B., Masson, D.G., Bett, B.J., 2002. Hydrodynamic significance of variable ripple morphology across deep-water barchan dunes in the Faroe-Shetland channel. Mar. Geol. 192, 309–319. https://doi.org/10.1016/S0025-3227(02)00561-3.
Wynn, R.B., Stow, D.A.V., 2002. Classification and characterisation of deep-water sediment waves. Mar. Geol. 192, 7–22. https://doi.org/10.1016/S0025-3227(02)00547-9.